SMC-TR-02-11

AEROSPACE REPORT NO.
TR-2000(8565)-11

Stress Measurements in Silicon Microstructures

January 2002

Prepared by

S. T. AMIMOTO, D. J. CHANG, and A. D. BIRKITT
Propulsion Science and Experimental Mechanics Department

Prepared for

SPACE AND MISSILE SYSTEMS CENTER
AIR FORCE MATERIEL COMMAND
2430 E. El Segundo Boulevard
Los Angeles Air Force Base, CA 90245

Engineering and Technology Group

THE AEROSPACE CORPORATION
El Segundo, California

This report was submitted by The Aerospace Corporation, El Segundo, CA 90245-4691, under Contract No. F04701-93-C-0094 with the Space and Missile Systems Center, 2430 E. El Segundo Blvd., Los Angeles Air Force Base, CA 90245. It was reviewed and approved for The Aerospace Corporation by P. D. Fleischauer, Principal Director, Space Materials Laboratory. M. Zambrana was the project officer for the Mission-Oriented Investigation and Experimentation (MOIE) program.

This report has been reviewed by the Public Affairs Office (PAS) and is releasable to the National Technical Information Service (NTIS). At NTIS, it will be available to the general public, including foreign nationals.

This technical report has been reviewed and is approved for publication. Publication of this report does not constitute Air Force approval of the report's findings or conclusions. It is published only for the exchange and stimulation of ideas.

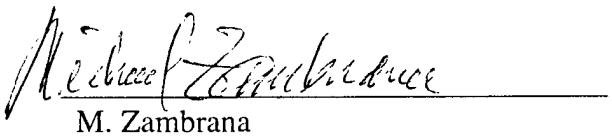

M. Zambrana
Project Officer

REPORT DOCUMENTATION PAGE

Form Approved
OMB No. 0704-0188

1. AGENCY USE ONLY (Leave blank)	2. REPORT DATE	3. REPORT TYPE AND DATES COVERED
	January 2002	

4. TITLE AND SUBTITLE
Stress Measurements in Silicon Microstructures

5. FUNDING NUMBERS
F04701-93-C-0094

6. AUTHOR(S)
S. T. Amimoto, D. J. Chang, and A. D. Birkitt

7. PERFORMING ORGANIZATION NAME(S) AND ADDRESS(ES)
The Aerospace Corporation
Technology Operations
El Segundo, CA 90245

8. PERFORMING ORGANIZATION REPORT NUMBER
TR-2000(8565)-11

9. SPONSORING/MONITORING AGENCY NAME(S) AND ADDRESS(ES)
Space and Missile Systems Center
Air Force Materiel Command
2430 E. El Segundo Blvd.
Los Angeles Air Force Base, CA 90245

10. SPONSORING/MONITORING AGENCY REPORT NUMBER
SMC-TR-02-11

11. SUPPLEMENTARY NOTES

12a. DISTRIBUTION/AVAILABILITY STATEMENT
Approved for public release; distribution unlimited

12b. DISTRIBUTION CODE

13. ABSTRACT (Maximum 200 words)

Raman spectroscopy is used as a noncontact probe of stress with high spatial resolution in micromachined silicon structures. The motivation for this work is that reliability or cycle life can be substantially increased by understanding the distribution of stress, including residual stress. High stresses induced by workmanship shortcomings or design constraints may be addressed by Raman measurements. In microelectronics, stress is known to play a significant role in interconnects, which limits reliability, life, and ultimately cost of many circuits. We wish to demonstrate the utility of Raman spectroscopy as a tool for the development and design of silicon microstructures.

The equations for a general two-dimensional stress field are discussed. Calibration studies using macro-mechanical fixtures for single crystal silicon specimens under two-dimensional stress field are presented. Our measurements show good agreement with the theoretical values and thus validate the approach taken. Stress maps of conventionally fabricated test structures, laser-machined structures, and polysilicon structures are presented.

14. SUBJECT TERMS	15. NUMBER OF PAGES
Raman spectroscopy, stress, stress field, micromachined silicon	13
	16. PRICE CODE

17. SECURITY CLASSIFICATION OF REPORT	18. SECURITY CLASSIFICATION OF THIS PAGE	19. SECURITY CLASSIFICATION OF ABSTRACT	20. LIMITATION OF ABSTRACT
UNCLASSIFIED	UNCLASSIFIED	UNCLASSIFIED	

ABSTRACT

Raman spectroscopy is used as a noncontact probe of stress with high spatial resolution in micromachined silicon structures. The motivation for this work is that reliability or cycle life can be substantially increased by understanding the distribution of stress including residual stress. High stresses induced by manufacturing flaws or design constraints may be addressed by Raman measurements. In microelectronics, stress is known to play a significant role in interconnects which limits reliability, life, and ultimately cost of many circuits. We wish to demonstrate the utility of Raman spectroscopy as a tool for the development and design of silicon microstructures.

The equations for a general two-dimensional stress field are discussed. Calibration studies using macromechanical fixtures for single crystal silicon specimens under a two-dimensional stress field are presented. Our measurements show good agreement with the theoretical values and thus validate the approach taken. Stress maps of conventionally fabricated test structures, laser machined structures, and polysilicon structures are presented.

Keywords: Raman spectroscopy, stress, stress field, micromachined silicon

ACKNOWLEDGMENTS

This work was performed under the support of a Mission Oriented Investigation and Experimentation project funded by the Air Force Space and Missile Systems Center (AFSMC) and a grant funded by the Directorate of Aerospace and Materials Sciences of the Air Force Office of Scientific Research (AFOSR).

Contents

Figures

1. INTRODUCTION

High stress levels play a significant role in determining the life, the reliability, and the failures of micromachined and microelectronic devices. High stresses due to coefficient of thermal expansion (CTE) mismatch and discontinuities have led to failures in interconnects and metallizations due to stress migration and electromigration effects. Stress in films may also cause adhesion failure between film layers. Fatigue life may be considerably shortened by the presence of localized high stress in critical regions. Structural designs, workmanship, and manufacturing methods including laser machining also play a role in determining stress. We have proposed Raman spectroscopy as a noncontact method for measuring highly localized stresses at the surface of silicon structures to understand the effects of macro- and micromaterial property variations, design, and defects as they influence stress concentrations. Raman spectroscopy has excellent spatial resolution of 1 μm and is well suited to probing the nanostructures used in MEMS devices. The stress measurement is based on the relative frequency shift of the Raman spectra when the crystal lattice is strained. Stresses as small as 8.7 MPa (1.25 ksi) may be detected.

This paper presents the Raman secular equation for cubic crystal systems and discusses the general, two-dimensional surface stress field effects on Raman frequency shifts and polarization. Raman stress measurements of single-crystal silicon test structures undergoing four-point bend loading are used to validate the theory. These are the first measurements reported for single crystal silicon undergoing tensile stress. Residual stress measurements in polysilicon cantilever beams and preliminary stress maps in laser machined test structures using the Revise Inc. (see Reference 1) process are also reported.

2. THE RAMAN EQUATIONS FOR CUBIC SYSTEMS

The Raman dynamic equations for optical modes in a cubic crystal were used to derive the stress dependent frequency shift relationships. The secular equation for a cubic crystal such as silicon is expressed

$$\begin{vmatrix} [pe_{xx} + q(e_{yy} + e_{zz}) - \lambda] & 2re_{xy} & 2re_{xz} \\ 2re_{xy} & [pe_{yy} + q(e_{xx} + e_{zz}) - \lambda] & 2re_{yz} \\ 2re_{xz} & 2re_{yz} & [pe_{zz} + q(e_{xx} + e_{yy}) - \lambda] \end{vmatrix} = 0 \quad (1)$$

where p, q, and r relate to the atomic spring constants for the crystal, the ε_{ij} are the strain components and $\lambda = \Omega^2 - \omega_o^2$ represents the frequency shift. Since λ is so much smaller than ω_o, the shifted frequency Ω can be approximated by $\Omega = \omega_o + \lambda/2\omega_o$ and $\Delta\Omega = \Omega - \omega_o = \lambda/2\omega_o$.

The two-dimensional stress field is appropriate to a surface where stress perpendicular to the surface is absent. Consider a general two-dimensional stress field τ_{11}, τ_{22}, and τ_{12} where τ_{11} and τ_{22} are two normal stresses in directions 1 and 2, respectively, and τ_{12} is the shear stress with respect to a Cartesian coordinate system with axes 1, 2, and 3. Further, let the 1, 2, and 3 axes coincide with the principal axes of the cubic crystal material with axis 3 normal to the surface. Let the three stress components be related by the parameters α and β as follows:

$$\tau_{11} = \tau, \ \tau_{22} = \alpha\tau, \text{ and } \tau_{12} = \beta\tau \quad (2)$$

The following three roots (frequency shifts) are derived from solving Eqn. (1):

$$\Delta\Omega_1 = (\tau/4\omega_o)\{p(1+\alpha)(S_{11} + S_{12}) + q(1+\alpha)(S_{11} + 3S_{12}) + [(1-\alpha)^2(S_{11} - S_{12})^2(p-q)^2 + 4(rS_{44}\beta)^2]^{1/2}\},$$

$$\Delta\Omega_2 = (\tau/4\omega_o)\{p(1+\alpha)(S_{11} + S_{12}) + q(1+\alpha)(S_{11} + 3S_{12}) - [(1-\alpha)^2(S_{11} - S_{12})^2(p-q)^2 + 4(rS_{44}\beta)^2]^{1/2}\},$$

$$\Delta\Omega_3 = (\tau/2\omega_o)\{p(1+\alpha)S_{12} + q(1+\alpha)(S_{11} + S_{12})\} \quad (3)$$

where S_{ij} are elements of the compliance matrix that relates stress to strain; p, q, and r are calibration constants; and ω_o is the reference frequency of unstressed silicon, 520 cm^{-1}. It is interesting to note that the root $\Delta\Omega_3$ is independent of the shear stress whereas the other two roots, $\Delta\Omega_1$ and $\Delta\Omega_2$ will show a splitting relative to each other that is shear and biaxial stress dependent. The values of $p/\omega_o^2 = -1.85$, $q/\omega_o^2 = -2.31$, $r/\omega_o^2 = -0.71$, $S_{11} = 7.68 \times 10^{-12}$ Pa^{-1}, $S_{12} = -2.14 \times 10^{-12}$ Pa^{-1}, and $S_{44} = 12.7 \times 10^{-12}$ Pa^{-1} were used for single crystal silicon (see Reference 2). For polycrystalline silicon (see Reference 3) the values are $p/\omega_o^2 = -1.40$, $q/\omega_o^2 = -2.00$, $r/\omega_o^2 = -0.67$, $S_{11} = 7.73 \times 10^{-12}$ Pa^{-1}, $S_{12} = -2.15 \times 10^{-12}$ Pa^{-1}, and $S_{44} = 12.7 \times 10^{-12}$ Pa^{-1}.

2.1 Transition Dipole Moments and Selection Rules

The three frequency shifts associated with the stress field are not necessarily observable simultaneously at a specific orientation. Their detectability depends on the combination of the polarization of the incident light and the scattered light. For cubic crystals such as silicon, the Raman tensors in the 1, 2, and 3 directions are respectively

$$R_1=\begin{bmatrix}0&0&0\\0&0&d\\0&d&0\end{bmatrix},\qquad R_2=\begin{bmatrix}0&0&d\\0&0&0\\d&0&0\end{bmatrix},\qquad R_3=\begin{bmatrix}0&d&0\\d&0&0\\0&0&0\end{bmatrix}$$

The Raman tensors corresponding to the three Eigenvectors under the above two-dimensional stress field are

$$\bar{R}_1=\frac{1}{\sqrt{1+\Delta_1^2}}\begin{bmatrix}0&0&\Delta_1 d\\0&0&d\\\Delta_1 d&d&0\end{bmatrix},\quad \bar{R}_2=\frac{1}{\sqrt{1+\Delta_2^2}}\begin{bmatrix}0&0&d\\0&0&\Delta_2 d\\d&\Delta_2 d&0\end{bmatrix},\quad \bar{R}_3=\begin{bmatrix}0&d&0\\d&0&0\\0&0&0\end{bmatrix}$$

where d is the lattice constant. Its magnitude is of the order of 10 nm. Δ_1 and Δ_2 are defined in Eqn. (5d)

Selection rules were examined by evaluating the dipole moment for the strain-induced Eigenvectors for the following polarizations of incident and scattered light. Let $\mathbf{e_i}$ and $\mathbf{e_s}$ be the incident and scattered light with polarizations of:

$$e_i^j=\begin{bmatrix}l_{i1}^j\\l_{i2}^j\\l_{i3}^j\end{bmatrix},\qquad e_s^j=\begin{bmatrix}l_{s1}^j\\l_{s2}^j\\l_{s3}^j\end{bmatrix}$$

where l_{km}^j are directional cosines and $(l_{k1}^j)^2+(l_{k2}^j)^2+(l_{k3}^j)^2=1 \quad k=i,s.$ (4)

The superscript j labels the three roots in (3). The scattering intensity of the Raman signal is defined as $C\Sigma\,|\mathbf{e}_i^j\,\bar{\mathbf{R}}_j\,\mathbf{e}_s^j|^2$ where C is a scalar constant. The results summarized below show the amplitude strength of the observed frequency shift for each solution in (3).

$$e_i^1\,\bar{R}\,e_s^1=l_{i3}^1(l_{s1}^1\Delta_1+l_{s2}^1)d/\sqrt{1+\Delta_1^2}, \tag{5a}$$

$$e_i^2\,\bar{R}\,e_s^2=l_{i3}^2(l_{s1}^2+l_{s2}^2\Delta_2)d/\sqrt{1+\Delta_2^2}, \tag{5b}$$

$$e_i^3\,\bar{R}\,e_s^3=(l_{i2}^3 l_{s1}^3+l_{i1}^3 l_{s2}^3)d. \tag{5c}$$

where

$$\Delta_1=\frac{(1-\alpha)(S_{11}-S_{12})(p-q)/2-D}{rS_{44}\beta},\quad \Delta_2=\frac{rS_{44}\beta}{(1-\alpha)(S_{11}-S_{12})(p-q)/2+D}, \tag{5d}$$

$$D=\frac{1}{2}\sqrt{(1-\alpha)^2(S_{11}-S_{12})^2(p-q)^2+4(rS_{44}\beta)^2}.$$

A strategy to uniquely identify the transitions from <001> single crystal silicon can be developed from the selection rules. It is seen from Eqn. (5) that for cases corresponding to backscatter from a <001> surface, only longitudinal phonons can be observed since only (5c) remains nonzero for polarizations in the x-y plane. When the polarization angles of incident light and the scattered light complement each other in backscatter from the <001> surface, the amplitude (5c) is maximized. When the incident and scattered polarizations are parallel ($\ell_{s3}^3=0$) and the polarization vectors are aligned with either the x or y axis in the backscatter configuration, all amplitudes become zero. The (5c) term is nonzero for all other polarization orientations. Hence its behavior can be used to determine the crystallographic orientation of the cubic crystal (see Reference 4).

In order to observe the effects of shear as expressed by $\Delta\Omega_1$ and $\Delta\Omega_2$, the sample must be tilted to allow a nonzero projection along the z-axis to allow non-vanishing ℓ^1_{i3} or ℓ^2_{i3}. In this tilted configuration, if the polarizations of the incident and scattered light are parallel, then the longitudinal phonon transition (5c) can be nulled to enable observation of only the first two roots. In general, as observed in the backward direction to the tilted incident beam, one will detect the sum of the transition intensities of (5a) and (5b). If the frequency difference between $\Delta\Omega_{(j=1)}$ and $\Delta\Omega_{(j=2)}$ is sufficiently large compared to the linewidth, then it will be very easy to identify each transition by a rotation of the polarization vector around the incident axis. One or the other transition intensity will go to zero at an angle determined by Δ_1. In general, the ease of identifying the transitions and shifts is dependent on how much biaxial- and shear-stress is present. The separation of the peak positions of $\Delta\Omega_1$ and $\Delta\Omega_2$ is equal to $\frac{\tau D}{\omega_0}$ where D is defined above. In principle, if there is knowledge of the frequency shifts of all three transitions and the polarization angle at which either (5a) or (5b) becomes zero, then it is possible to derive the values of τ, α, and β.

3. EXPERIMENTAL SETUP

In the Raman stress experimental setup, a monochromatic light or laser shines on the surface of a specimen through a microscope. The specimen sits on a translation stage whose motion is controlled through a micrometer. The Raman scattered light is analyzed with a spectrometer. When the specimen is unstressed, the spectrometer measures a reference spectrum whose center position is that of the unstressed sample. When the specimen is placed in a stressed state, the spectrum will show a frequency shift that varies linearly with the applied stress. The measurements are conducted using an argon ion laser with a wavelength of 488 nm. The diameter of the laser spot is typically 1 to 2 μm with an estimated penetration depth for the incident light of 0.6 μm. The Raman spectra were least-square fitted with a Lorentzian profile to determine the center frequency shift.

The specimens that were used in the experimental tests included both calibration and MEMS specimens. The calibration specimen was a piece of single crystal silicon in a strip configuration. The strip specimen was either clamped or simply supported at its two end regions. The specimens had a clear central span L and were loaded with two rollers located symmetrically with respect to the center of the specimen. Loads in the samples were induced by turning the set screw located at the center of the supported strip. The magnitude of the load setting was recorded from the load cell. The maximum surface stress of the sample between the central supports is:

$$\sigma_s = 3Pb^2/(Lwt^2) \tag{6}$$

for the clamped sample and for the simply supported sample is:

$$\sigma_s = 3Pb/(wt^2) \tag{7}$$

where P is the total load measured by the load cell, b and L are the dimensions shown in Figure 1, and w and t are the width and thickness, respectively, of the strip.

Strip samples of <001> single crystal silicon were fabricated from 3-inch diameter standard n-type single crystal silicon wafers for use in either fixture. The sample dimensions were 12.7-mm (0.500 in.) in width and 0.394-mm (0.0155 in.) in thickness. They consist of two types such that a unidirectional stress could be applied either in the (110) or (100) directions.

The calculated results for single crystal silicon using (2) relate the Raman shifts in units of cm^{-1} to stress σ in units of Pascals as follows:

For applied uniaxial stress along the (100) direction, $\tau = \sigma_s = \sigma$, $\alpha = 0$ and $\beta = 0$: $\Delta\Omega_3 = -2.3 \times 10^{-9}\sigma_s$.

For applied uniaxial stress along the (110) direction, $\tau = \sigma_s/2 = \sigma/2$, $\alpha = 1$ and $\beta = 1$: $\Delta\Omega_3 = -2.3 \times 10^{-9}\sigma_s$.

The calculated results for polysilicon using (2) relate the Raman shifts in units of cm^{-1} to stress τ in units of Pascals as follows:

For "normal" uniaxial stress, $\alpha = 0$ and $\beta = 0$: $\Delta\Omega_3 = -2.12 \times 10^{-9}\tau$.

For "normal" equal biaxial stress without shear, $\alpha = 1$ and $\beta = 0$: $\Delta\Omega_3 = -4.24 \times 10^{-9}\tau$.

The term "normal" refers to stress components in the same direction as the crystal axis. The latter case may correspond to stress caused by a mismatch in the coefficient of thermal expansion between two adjacent layers.

The MEMS specimen is a cantilever beam fabricated by the MUMPS process (see reference 5). Its nominal dimensions are 200μm long, 20μm wide, and 2μm thick. It simulates an electrical relay. Since polysilicon is partially conductive, an insulating oxidation layer was deposited between the cantilever

and the ground to allow application of a voltage that induces an electrostatic force in the cantilever. When the voltage increases to a critical value, the cantilever beam will collapse onto the ground. The deformation induced by the voltage will generate bending stresses in the beam with maximum values at the clamped end. Figure 2 shows a photograph of a set of three cantilever beams.

Simple test structures were fabricated from <100> single crystal silicon using a Revise Inc. (see reference 6) laser machining work station. The process uses thermal heating by a laser to enhance chemical etch rates in an atmosphere of chlorine gas. A resolution of 2 μm is possible when the laser beam is focused well. Square-shaped trenches were fabricated by raster scanning the laser spot at a power of a few watts with the 514.5 and 488.0-nm wavelengths from an Ar ion laser.

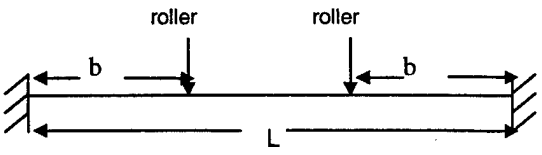

Figure 1. Schematics of a strip specimen in a fixture for either a clamped or simply supported end.

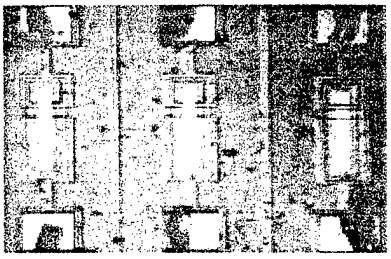

Figure 2. Photograph of MEMS cantilever beams fabricated by MUMPS process.

4. RESULTS AND DISCUSSION

Figure 3 depicts the Raman spectra of wafer cut from an annealed single crystal silicon boule. The average center frequency shift measured at random locations on the wafer is 520.28 $\pm$ 0.06-cm^{-1} at room temperature. This uncertainty should correspond only to a uniaxial stress with no shear component with a value of $\pm$ 26-MPa (or $\pm$3.8-ksi). The estimated error in the determination of the fitted line position is 0.02-cm^{-1} or 8.7-Mpa (1.25-ksi). Measurements were also taken on an annealed polysilicon layer deposited on a SiO_2 layer on top of a single-crystal silicon substrate in Figure 4. These measurements showed a spatial variability of $\pm$ 68.3-MPa (9.8-ksi) which is well in excess of the residual stress of the uncoated substrate, indicating that the coating has increased the residual stress. This finding is consistent with the earlier work of Miura (see Reference 7).

Raman frequency measurements for <001> single crystal silicon strip with (100) applied unidirectional stress are presented in Figure 5. The measured slope is 2.86 $\pm$ 0.27 x 10^{-9}-cm^{-1}/Pa. The theoretical slope is 2.3 x 10^{-9}-cm^{-1}/Pa. The Raman frequency measurements with (110) applied unidirectional stress are presented in Figure 6. This sample and its stress orientation correspond to the equal biaxial case discussed above. The measured slope is 2.07 $\pm$ 0.14 x 10^{-9}-cm^{-1}/Pa compared to the expected value of 2.3 x 10^{-9}-cm^{-1}/Pa. The agreement for both types of samples is within 20% of theory and is within the 2-sigma error bounds of the data. While these data provide the necessary calibration and confirmation of the theoretical and experimental approach taken in this paper further refinements of the measurements and reduction of experimental uncertainties are in progress.

In Figure 7, a preliminary residual stress map for a polysilicon cantilever beam is presented for the critical region of the beam near the support. Locations of the measurements are indicated in the figure. Large compressive stresses were observed despite the factor of 2 uncertainty that arises from whether the stress is uniaxial or biaxial. The measurements were taken near a discontinuity in layered films of dissimilar thermal expansion coefficients. Further study is required to resolve the stress into its components for this geometry. Preliminary stress profiles in terms of frequency shifts near the edge of a 0.20-mm square, 28-μm deep trench fabricated using the Revise Inc. laser-enhanced (thermal) chlorine etch are shown in Figure 8. The square trench was well isolated, greater than 0.5 mm from other trench structures fabricated on the same wafer. The laser has a spot size of 2-μm and power of a few watts. While some variation on the order of a few tenths of a cm^{-1} occurs due to residual stress associated with processing defects in the substrate, the fabrication of the trench has caused large stresses. Relative to the outside of the trench, a large negative shift of 1.9-cm^{-1} is observed inside the trench. This indicates that the floor of the trench has less compressive stress (or more tensile).

We have not performed the measurements to determine whether the shift is due to a simple uniaxial stress or some combination of (biaxial) stresses. The single measurement reported is also insensitive to shear contributions. The simplest assumption is the case of only uniaxial stress. More work is needed to fully determine the contributions from all of the full stress tensor terms. Assuming this is due only to a uniaxial stress, the stress difference is 830-MPa. The magnitude of this stress is sufficiently large to cause significant concern for the mechanical reliability of parts using this fabricated trench approach. In addition, at the outer and inner edges of the trench wall sharp stress gradients can be observed, causing additional concern. The origin of the stresses may be due to stress concentration caused by the discontinuity of the edge of the trench or to heating by the laser to cause compressive yielding. Further experiments are required to identify the mechanism responsible.

5. SUMMARY

In summary, we have demonstrated analytically that the two-dimensional surface stresses normal to the <001> plane of a cubic crystal have a unique relationship with the Raman frequency shifts. In other words, for a cubic crystal whose spring constants p, q, r are known, once the Raman frequency shifts and polarization characteristics are measured, then the associated surface stress components can be determined. We have also demonstrated that the measured Raman frequency shifts for a single crystal silicon under unidirectional tensile stress in both (110) and (100) directions agree well with analytical predictions. With this validation in hand, Raman spectra can be used to address the role of stress for reliability assessments and failure mechanisms in MEMS and microelectronics. The use of these Raman stress diagnostics will lead to improved lifetimes, the identification of defects, and improved fabrication for future silicon devices. In this work, high stress levels were observed in simple single- and poly-crystalline samples that raise concern for deleterious effects for these types of structures.

In order to be able to describe the stress field completely, both shear stresses and normal stresses must be measured. At this time, the technique for measuring shear stresses has yet to be developed, although the theoretical background for doing so has been worked out (see Reference 8). The Raman measurements will provide the maximum benefits in stress characterization for silicon-type MEMS systems when the entire stress field can be derived from the Raman spectra.

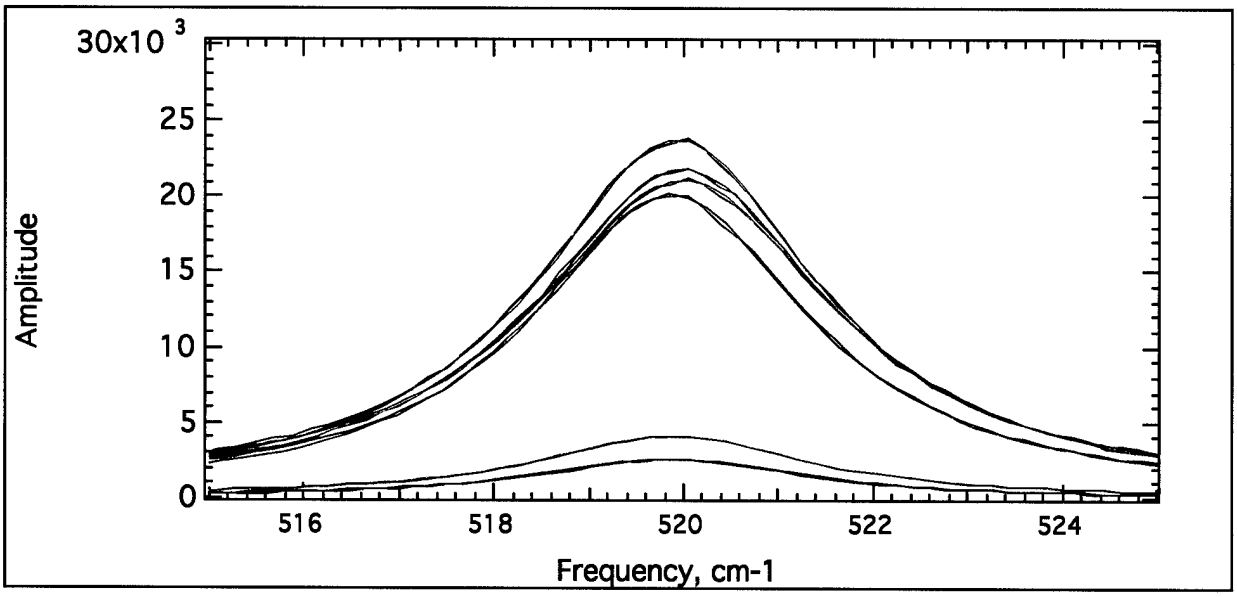

Figure 3. Raman spectra for unstressed, single-crystal Si (data collected at different locations).

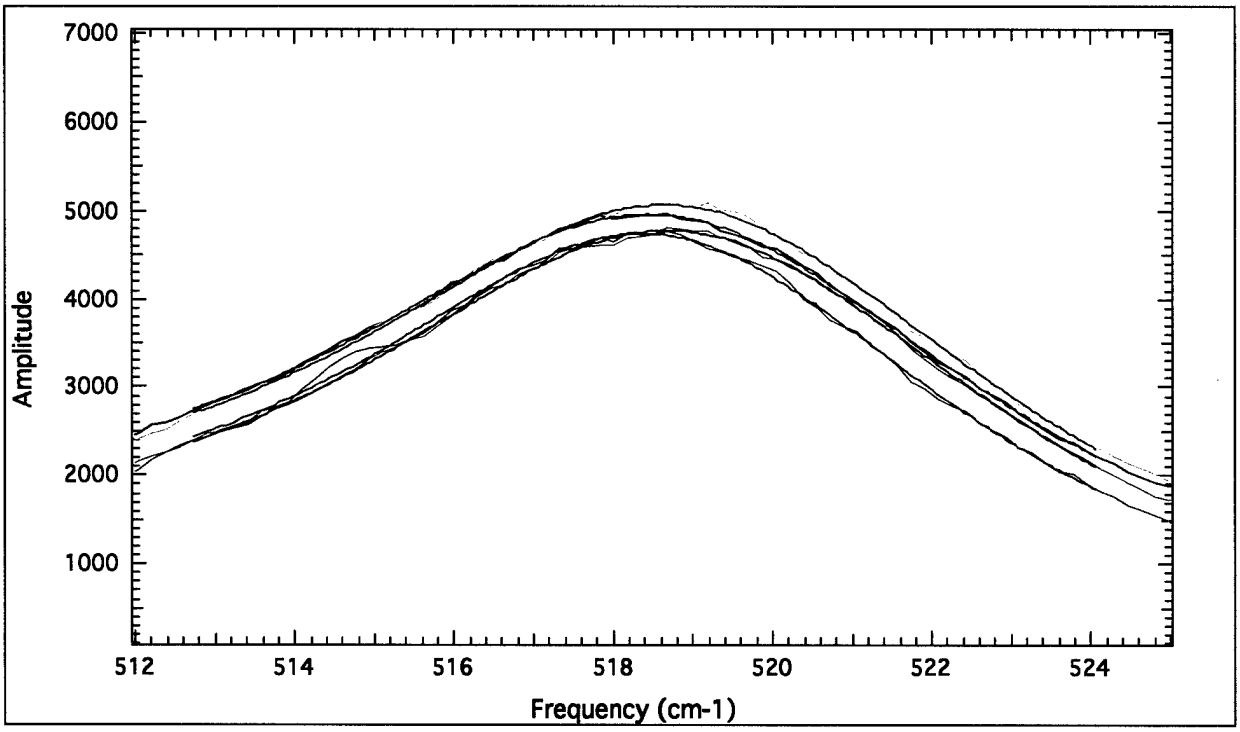

Figure 4. Raman spectra for polysilicon deposited on SiO_2 on single crystal Si substrate at different locations.

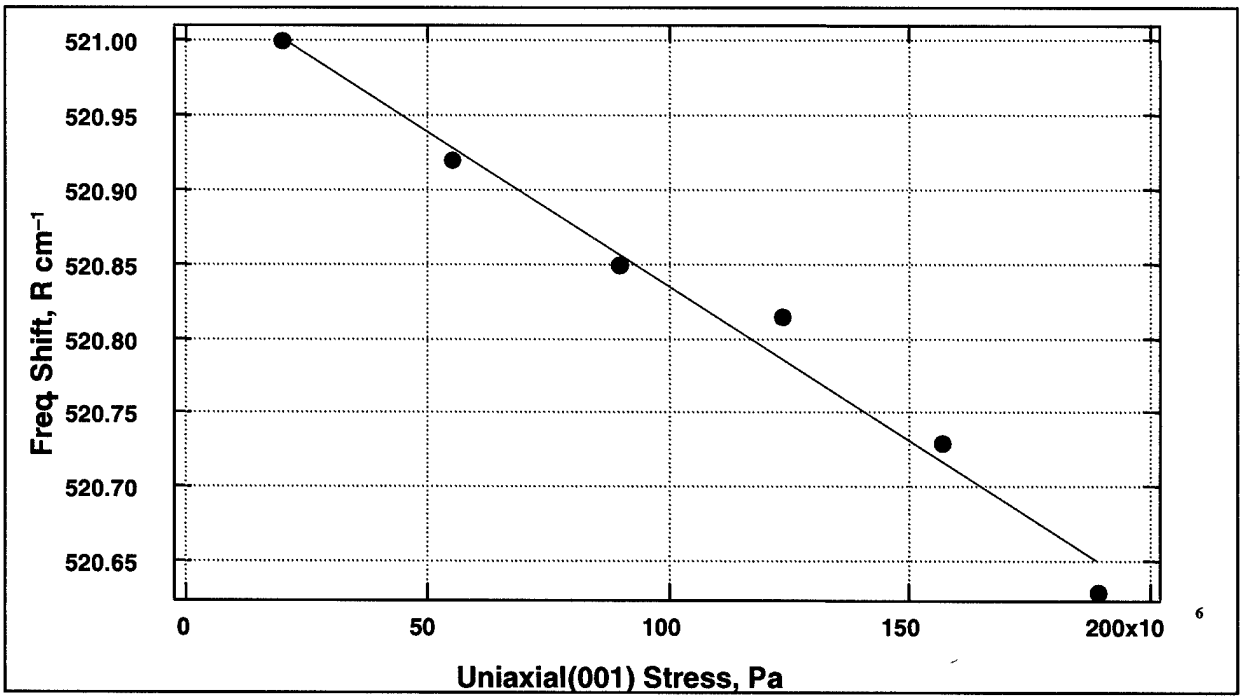

Figure 5. Frequency shift as a function of external uniaxial applied stress in the (100) direction.

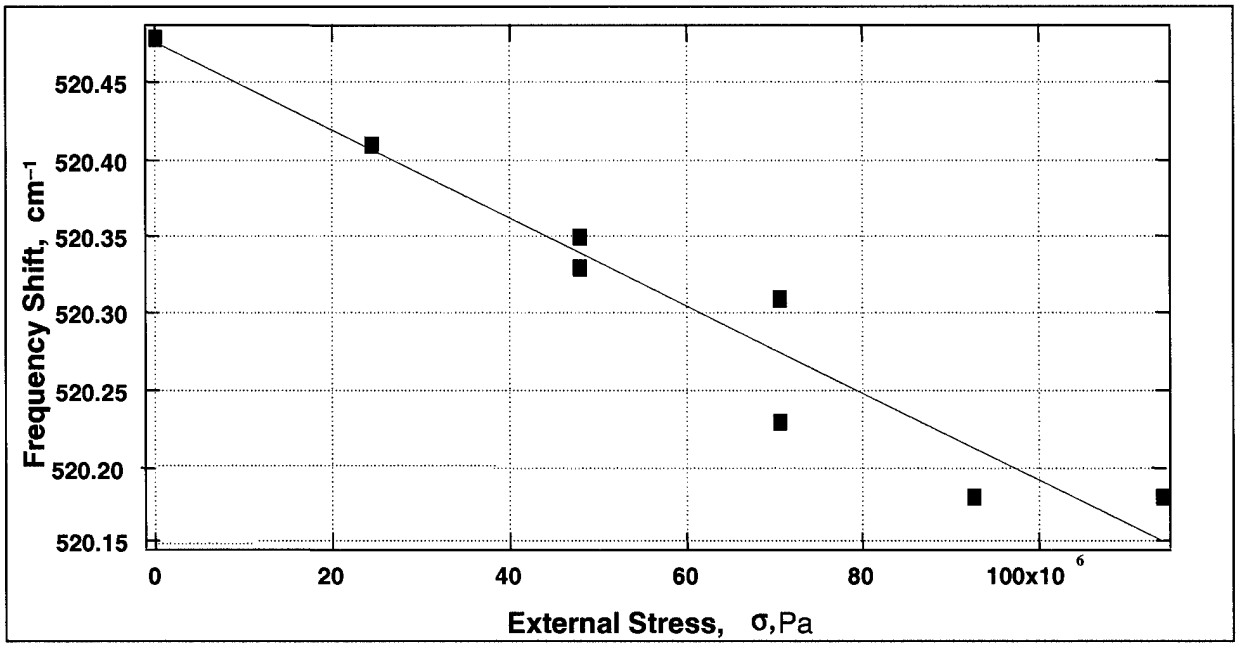

Figure 6. Frequency shift as a function of applied external uniaxial stress in the (110) direction.

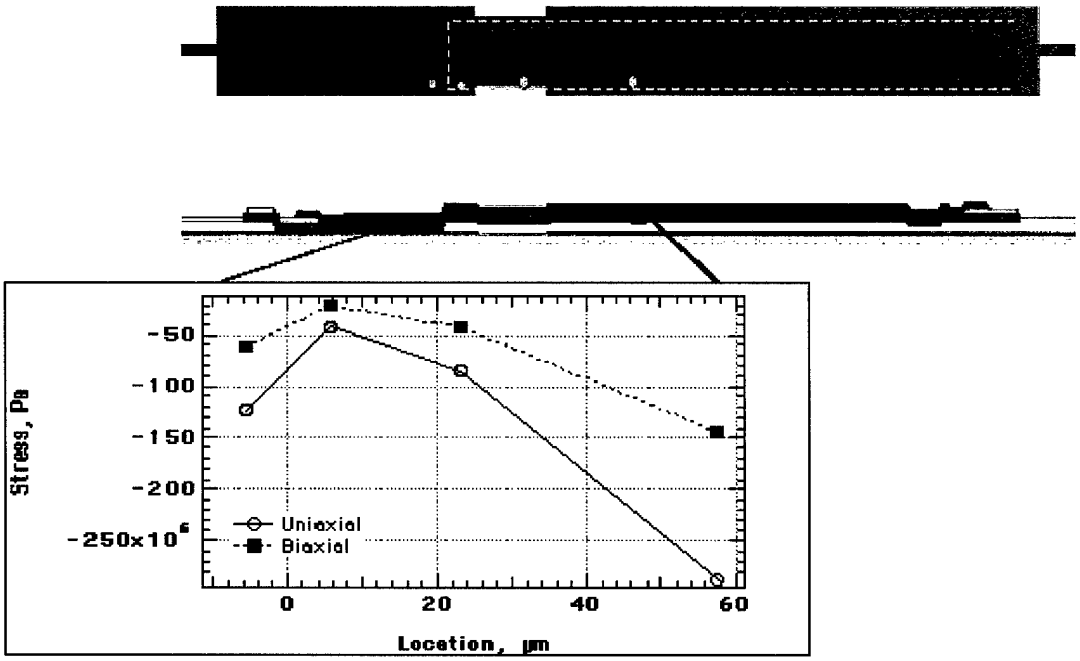

Figure 7. Stress map of a 20 x 200 µm polysilicon (dashed lines) cantilever beam.

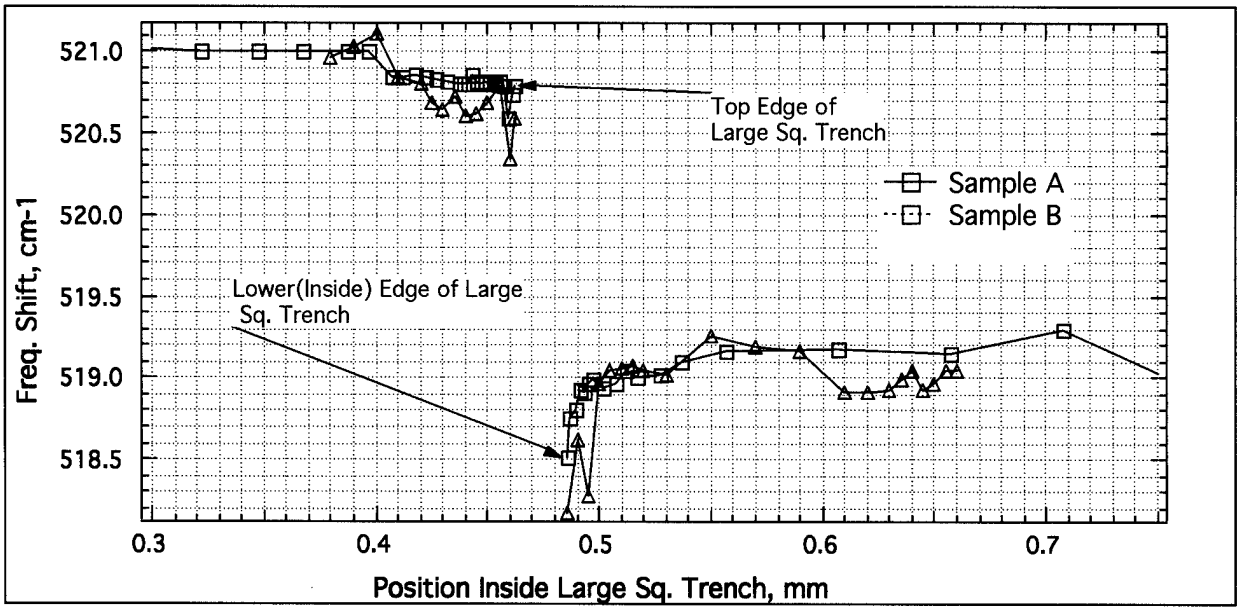

Figure 8. Stress profiles near the edges of two sample specimens of a 0.20-mm square trench.

REFERENCES

1. J. G. Black, D. J. Erlich, M. Rochschild, S. P. Doran, and J. H. C. Sedlecek, "Laser-direct-writing processes: Metal deposition, etching and applications to microcircuits," *J. Vac. Sci. Technol.* B 5 (1), Jan/Feb 1987.
2. E. Anastassakis, A. Cantarero, and M. Cardona, "Piezo-Raman measurements and anharmonic parameters in silicon and diamond," *Phys. Rev. B* **41**, pp. 7529-7535, 1990; E. Anastassakis, A. Pinczuk, E. Bernstein, F. H. Pollak, and M. Cardona, "Effect of static uniaxial stress on the Raman spectrum of silicon," *Sol. State Comm.* **8**, pp. 133-138, 1970.
3. E. Anatassakis and E. Liarokapis, "Polycrystalline Si under strain: Elastic and lattice-dynamical consideration," *J. Appl. Phys.* **62**, pp. 3346-3352, 1987
4. G. Kolb, T. Salbert, and G. Arstreiter, "Raman-microprobe study of stress and crystal orientation in laser crystallized silicon", *J. Appl. Phys.* **69**, pp. 3387-3389, 1991.
5. *MUMPS or Multi-User MEMS Processes at the MEMS Technology Application Center*, MCNC, 3021 Cornwallis Rd, Research Triangle Park, NC 27709.
6. This process is described in T. M. Bloomstein and D. J. Erhlich, "Stereo laser micromachining of silicon", *J. Vac. Sci. Technol. B*, 2671(1992)
7. H. Miura, H. Sakata, and S. Sakata, "Residual stress measurement of Si substrates after thermal oxidation using microscopic Raman spectroscopy," *Proceedings of the 9th International Conference on Experimental Mechanics*, 20-24 August 1990, Copenhagen, Denmark, pp. 1301-1306.
8. D. J. Chang, S. T. Amimoto, and A. D. Birkitt, *Research in Mechanics of MEMS Devices*, Aerospace TR-99(8565)-3, 10, September, 2000.